Konrad-Zuse-Zentrum
für Informationstechnik Berlin

Takustraße 7
D-14195 Berlin-Dahlem
Germany

L. ZSCHIEDRICH, R. KLOSE, A. SCHÄDLE, F. SCHMIDT

A new Finite Element realization of the Perfectly Matched Layer Method for Helmholtz scattering problems on polygonal domains in 2D

ZIB-Report 03-44 (December 2003) (revised version December 2004)

A New Finite Element Realization of the Perfectly Matched Layer Method for Helmholtz Scattering Problems on Polygonal Domains in 2D

Lin Zschiedrich, Roland Klose, Achim Schädle, and Frank Schmidt

Konrad-Zuse-Zentrum Berlin, Takustr. 7, D-14195 Berlin-Dahlem.
Revised Version December 2004

Abstract

In this paper we propose a new finite element realization of the Perfectly Matched Layer method (PML-method). Our approach allows to deal with a wide class of polygonal domains and with certain types of inhomogeneous exterior domains. Among the covered inhomogeneities are open waveguide structures playing an essential role in integrated optics. We give a detailed insight into implementation aspects. Numerical examples show exponential convergence behavior to the exact solution with the thickness of the PML sponge layer.

Key words: transparent boundary conditions, perfectly matched layer, pole condition

1 Introduction

Scattering problems arising from integrated optics are modeled by Maxwell's equations on unbounded domains. Typically waveguide structures connect various sub-components over a distance of a large number of wavelengths. A central task in the numerical solution of such problems is the implementation of transparent boundary conditions, which is often realized by Bérenger's Perfectly Matched Layer method (PML-method) [1–4]. Monk and Collino [5] introduce the PML-method in a homogeneous medium for separable coordinate systems as a complex continuation in one distance variable by exploiting the analyticity of the solution. For this case Lassas et al. prove the exponential convergence of the PML-method [6]. By introducing a normal tangential coordinate system they extend these results to general convex domains [7].

This coordinate system is defined by a parameterization of the boundary (τ variable) and the Euclidian distance ν from the boundary, cf. Fig. 1. Their proof for the convergence of the PML-method in a homogeneous medium is based on a complex continuation in ν-direction. A numerical realization of the PML method based on a normal tangential is proposed in [8]. However in typical applications from integrated optics, see Fig. 1, the solution may only be analytic in a direction different from ν. In Fig. 1 the sketched waveguide cuts the τ-isolines. Hence the solution is not analytic in ν-direction.

In this paper we propose a new realization of the PML-method by introducing coordinate systems which we call prismatoidal. This yields a clear concept on a semi-discrete level. Our approach allows a flexible adaption to many geometries, even with inhomogeneous exterior domains, cf. Fig. 2. In contrast to [9] the definition of a complex Riemann metric on a continuous level is avoided. We restrict ourselves to the two dimensional case for the sake of a clear presentation of the underlying concept. The ideas carry over to the three dimensional case and to the vectorial Maxwell equations [10] as we will present in a future paper.

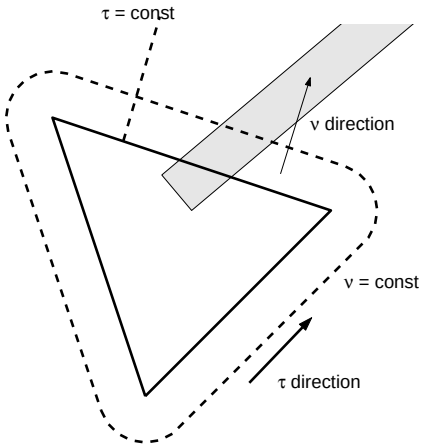

Fig. 1. Normal-tangential coordinate system used by Lassas et. al. The waveguide structure yields solutions not analytic in ν-direction.

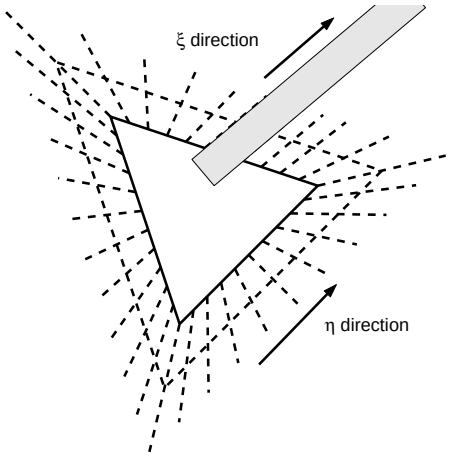

Fig. 2. Prismatoidal coordinate system. The waveguide structure yields solutions analytic in ξ-direction.

Maxwell's time harmonic equations for a source and current free medium lead to the photonic wave equations. We consider the two dimensional case. For TE-polarization the H-field takes the form $(0, 0, H_z)$, and the first photonic wave equation reads

$$\nabla \cdot \left(\frac{1}{\epsilon(x,y)} \nabla H_z(x,y) \right) + \frac{\omega^2}{c^2} H_z(x,y) = 0. \tag{1}$$

For TM-polarization the E-field takes the form $(0, 0, E_z)$, and the second pho-

tonic wave equation reads

$$\Delta E_z(x,y) + \frac{\omega^2}{c^2}\epsilon(x,y)E_z(x,y) = 0. \tag{2}$$

In the sequel we deal with the case of TM-polarization. The unbounded domain is divided into an inner domain Ω and an exterior domain Ω_{ext}. On the common boundary of the interior and the exterior domain, the field u separates into a given incoming field u_{inc} and a scattered field u_s. The scattering problem is determined by

$$\begin{aligned}
\Delta u(\boldsymbol{x}) + k^2(\boldsymbol{x})u(\boldsymbol{x}) &= 0 \quad \text{in } \Omega, && (3)\\
\Delta u_s(\boldsymbol{x}) + k^2(\boldsymbol{x})u_s(\boldsymbol{x}) &= 0 \quad \text{in } \Omega_{ext}, && (4)\\
u(\boldsymbol{x}) &= u_{inc}(\boldsymbol{x}) + u_s(\boldsymbol{x}) \quad \text{on } \partial\Omega, && (5)\\
\partial_\xi u(\boldsymbol{x}) &= \partial_\xi u_{inc}(\boldsymbol{x}) + \partial_\xi u_s(\boldsymbol{x}) \quad \text{on } \partial\Omega. && (6)
\end{aligned}$$

Here ξ denotes the non-tangential coordinate of the prismatoidal coordinate system described in Section 2. The scattered field has to satisfy a radiation condition at infinity. For homogeneous exterior domains this is the Sommerfeld radiation condition [11],

$$\lim_{r\to\infty} r^{\frac{d-1}{2}} \left(\frac{\partial u}{\partial r} - iku\right) = 0. \tag{7}$$

For $d > 1$ this implies that the field decays uniformly for all directions $\hat{x} = x/\|x\|$. Further the field is an outgoing monochromatic wave. For inhomogeneous exterior domains the Sommerfeld radiation condition does not hold true. For example regard an exterior domain such as depicted in Fig. 1. A straight waveguide with local wavenumbers k_1 ranges from the interior domain to infinity. Such a structure guides eigenmodes without damping in the direction of the waveguide. These types of solutions do not exist for homogeneous equations, since the Sommerfeld radiation condition implies the decay of the fields. Furthermore a waveguide may support a couple of eigenmodes with different propagation constants.

F. Schmidt proposes a general concept called pole condition to define radiation conditions for scattering problems [12]. In [13] it is shown that the pole condition is equivalent to the Sommerfeld radiation condition for homogeneous exterior domains. The pole condition leads to new algorithms to construct transparent boundary conditions [12]. Further it gives a new insight to PML. In [14] Hohage et al. prove the convergence of the PML-method for separable but inhomogeneous exterior domains. The aim of this paper is to propose a new finite element realization of the PML-method which is based on the theoretical concepts given in [12]. We do not aim to prove existence and uniqueness of the sought solutions. However various numerical examples indicate experimental convergence of the method.

2 Local prismatoidal coordinate systems in two dimensions

This section summarizes geometrical aspects of the pole condition approach [12], which are the basis for the proposed realization of the PML method. The central idea is to decompose the exterior domain into a finite number of segments and to associate with each segment a local coordinate system, such that a global distance variable ξ can be introduced. We realize the PML-method as a complex continuation along the ξ- direction. This is analogous to the approach by Collino and Monk [5] for global separable coordinate systems. Our approach resembles the definition of a global normal-tangential coordinate system in [7]. We stress the flexibility and the easy way of implementation of the method in the finite element context. The decomposition of the exterior

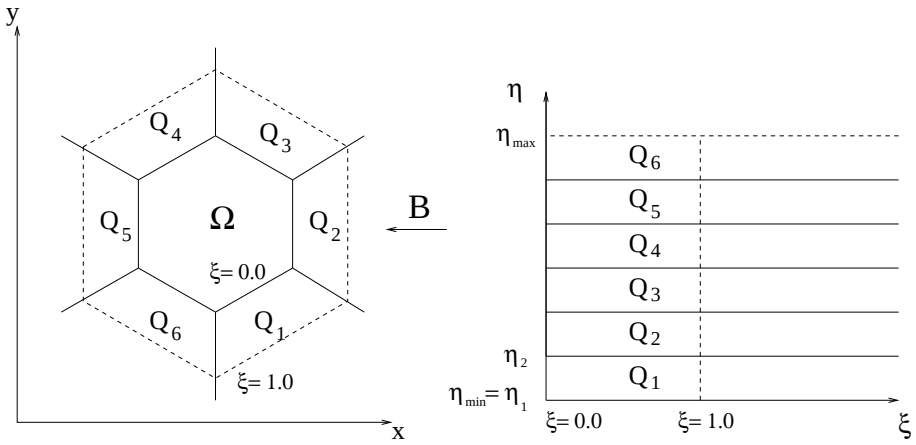

Fig. 3. Prismatoidal coordinate system. Each segment Q_j is the image of a reference element under a bilinear mapping B_j^{loc}. These local mappings are combined to a global mapping B which is continuous in η.

domain into a finite number of segments is based on straight non-intersecting rays $\boldsymbol{g}_j$, which connect each vertex $\boldsymbol{p}_j$ $(j = 1, ..., N)$ of the polygonal boundary $\partial\Omega$ with infinity. The set of rays together with the boundary $\partial\Omega$ generate a decomposition $\mathcal{L} = \{Q_1, ..., Q_N\}$ of $\overline{\Omega_{ext}}$. The constructed segments Q_j must be convex semi-infinite quadrilaterals.

We define a relation between the $\xi\eta$-coordinate system of a reference rectangle and the xy-coordinate system of each rectangle Q_j (cf. Fig. 3). For each Q_j we construct a bilinear transformation

$$B_j^{loc} : Q_j^{(\xi,\eta)} \rightarrow Q_j^{(x,y)} \tag{8}$$

from $Q_j^{(\xi,\eta)} := [0, \infty] \times [\eta_j, \eta_{j+1}]$ onto Q_j, such that the images of two lines $\xi_1 \times [\eta_j, \eta_{j+1}] \subset Q_j^{(\xi,\eta)}$ and $\xi_2 \times [\eta_j, \eta_{j+1}] \subset Q_j^{(\xi,\eta)}$ remain parallel under B_j^{loc}. This is possible due to the convexity of $Q_j^{(x,y)}$. In the following we define a prismatoidal coordinate system, whereas the name is chosen in accordance

with a future definition in three dimensions.

Definition 1 (Prismatoidal coordinate system) *Let Ω be a domain with polygonal boundary. Each vertex $\boldsymbol{p}_j$ of $\partial\Omega$ is connected with a straight ray $\boldsymbol{g}_j$, such that the set of rays is non-intersecting and a decomposition of Ω_{ext} into a finite number of convex semi-infinite segments Q_j is generated. The local bilinear mappings B_j^{loc} (8) associated with the segments Q_j are combined to a global transformation*

$$B : \overline{\Omega_{ext}^{(\xi,\eta)}} \to \overline{\Omega_{ext}^{(x,y)}}, \tag{9}$$

such that B is continuous and periodic in η with respect to $[\eta_{min}, \eta_{max}]$. The Jacobian of B is denoted by J.

Note that B is linear in ξ for fixed η. We give two different ways to construct prismatoidal coordinate systems [12].

Example 2 (Radial Rays) *Let a nonempty convex polygonal domain be given. Connect a fixed arbitrary interior point by line segments with each of the vertices of the boundary. Extend these line segments to linear rays. These rays define a prismatoidal coordinate system, cf. Fig. 4.*
For a star-shaped non-convex polygonal domain there exists by definition at least one interior point such that any line segment which connects this point with a vertex of the boundary hits the boundary only at this vertex. The line segments defined this way lead to a prismatoidal coordinate system, cf. Fig. 5.

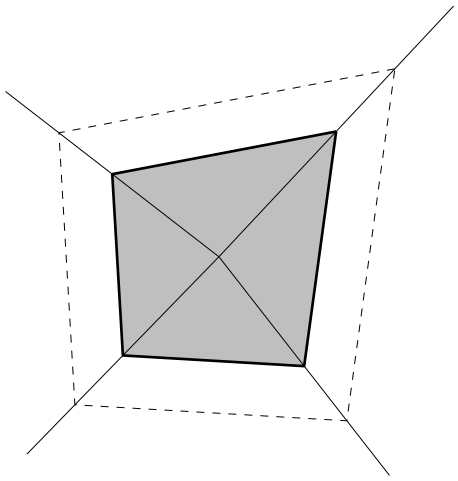

Fig. 4. Radial ray construction for convex domains.

Example 3 (Generalized normal rays) *Given a nonempty convex polygonal domain. Suppose that the vertices $\boldsymbol{p}_j$ of the polygonal boundary are numbered counter-clockwise from 1 to N_V. Choose rays $\boldsymbol{g}_j$, $j = 1, \ldots, N_V - 1$, corresponding to all but the last vertex $\boldsymbol{p}_{N_V}$ such that they have a representation $\boldsymbol{g}_j(\tau) = \boldsymbol{p}_j + \tau(c_i\boldsymbol{e}_i + c_k\boldsymbol{e}_k)$ with $\tau \in \mathbb{R}_+$ and both c_i and c_k strictly negative. The unit vectors $\boldsymbol{e}_i$ and $\boldsymbol{e}_k$ are given by $\boldsymbol{e}_i = (\boldsymbol{p}_i - \boldsymbol{p}_j)/|\boldsymbol{p}_i - \boldsymbol{p}_j|$ and*

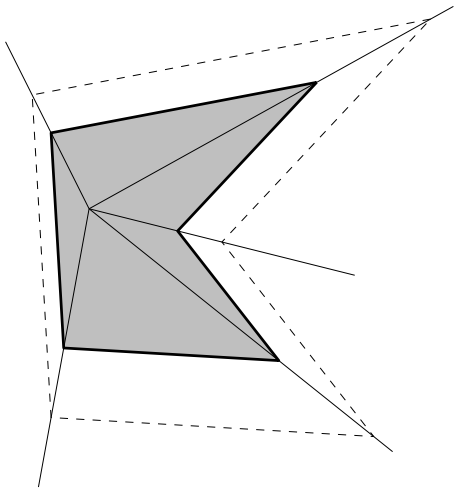

Fig. 5. Radial ray construction for star-shaped concave domain.

$\boldsymbol{e}_k = (\boldsymbol{p}_k - \boldsymbol{p}_j)/|\boldsymbol{p}_k - \boldsymbol{p}_j|$, *where* $\boldsymbol{p}_i$ *and* $\boldsymbol{p}_k$ *are the neighboring vertices to* $\boldsymbol{p}_j$. *The last ray* $\boldsymbol{g}_{N_V}$ *is constructed according to the following rule:*

(1) Fix an arbitrary point $\boldsymbol{q}_1$ *on ray* $\boldsymbol{g}_1$.
(2) Construct the two lines $\boldsymbol{s}_1$ *and* $\boldsymbol{s}_{N_V}$ *through this point, which are parallel to the neighboring boundary segments. (* $\boldsymbol{s}_1 || \overline{\boldsymbol{p}_1\boldsymbol{p}_2}$, $\boldsymbol{s}_{N_V} || \overline{\boldsymbol{p}_1\boldsymbol{p}_{N_V}}$*)*
(3) For $j = 2, \ldots, N_V - 1$ *the point* $\boldsymbol{q}_j$ *is the intersection of* $\boldsymbol{s}_{j-1}$ *with ray* $\boldsymbol{g}_j$ *and* $\boldsymbol{s}_j$ *is the parallel to the boundary segment* $\overline{\boldsymbol{p}_j\boldsymbol{p}_{j+1}}$ *through* $\boldsymbol{q}_j$.
(4) $\boldsymbol{g}_{N_V}$ *then is the ray from* $\boldsymbol{p}_{N_V}$ *through the intersection of* $\boldsymbol{s}_{N_V-1}$ *and* $\boldsymbol{s}_{N_V}$.

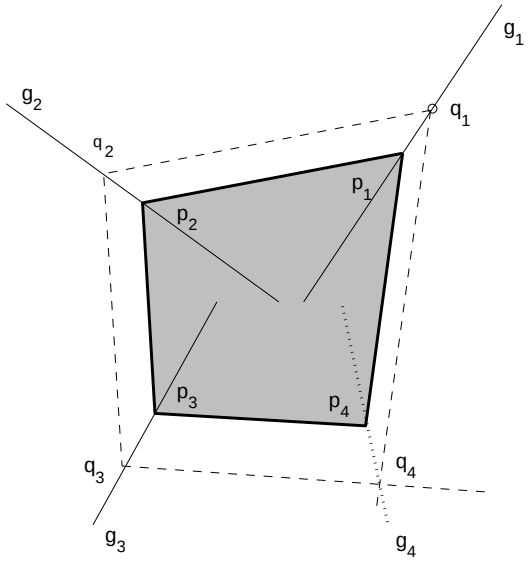

Fig. 6. Generalized normal ray construction for convex domains.

3 Semi-discretization based on local prismatoidal coordinate systems

In this section we introduce the semi discretization of the Helmholtz equation in the angular like variable η based on the local prismatoidal coordinate systems from Section 2. This is our general framework for different realizations of transparent boundary conditions such as the pole condition or the PML method.

The discrete form of the weak interior problem reads: Seek $u^h \in V_h \subset H^1(\Omega)$ such that for all $v^h \in V_h$

$$\int_\Omega \nabla u^h(\boldsymbol{x}) \cdot \nabla v^h(\boldsymbol{x}) \mathrm{d}\boldsymbol{x} - \int_\Omega k^2(\boldsymbol{x}) u^h(\boldsymbol{x}) v^h(\boldsymbol{x}) \mathrm{d}\boldsymbol{x} = \int_{\partial\Omega} \partial_n u^h(\boldsymbol{x}) v^h(\boldsymbol{x}) \mathrm{d}s. \quad (10)$$

The exterior problem can be formulated in the $\xi\eta$-coordinate system. The transformed Helmholtz equation is given by

$$\nabla_{\xi,\eta} \cdot (J^{-1}J^{-T}|J|\nabla_{\xi,\eta}) u_s + |J|k^2 u_s = 0. \quad (11)$$

Here we use the transformation rule for the gradient ∇_{xy} in x, y coordinates to the gradient $\nabla_{\xi\eta}$ in the local prismatoidal coordinates ξ, η. We assume a segment-wise constant wave number k. This ensures analyticity of the scattered field u_s in ξ-direction which is a necessary condition for an application of the PML-method [6]. Nevertheless enough flexibility is left for the configuration of the exterior domain by a proper choice of the segments. With $F := J^{-1}J^{-T}|J|$, Γ_η the part of $\partial\Omega$, where we impose the transparent boundary condition, and

$$\begin{aligned}
a_2(v, \partial_{\xi\xi} u_s) &= \int_{\Gamma_\eta} v F_{11} \partial_{\xi\xi} u_s \mathrm{d}\eta, \\
a_1(v, \partial_\xi u_s) &= \int_{\Gamma_\eta} v \partial_\xi F_{11} \partial_\xi u_s \mathrm{d}\eta - \int_{\Gamma_\eta} (\partial_\eta (v F_{12}) + (\partial_\eta v) F_{21}) \partial_\xi u_s \mathrm{d}\eta, \\
a_0(v, u_s) &= \int_{\Gamma_\eta} v \partial_\xi F_{12} \partial_\eta u_s \mathrm{d}\eta - \int_{\Gamma_\eta} \partial_\eta v F_{22} \partial_\eta u_s \mathrm{d}\eta + \int_{\Gamma_\eta} v |J| k^2 u_s \mathrm{d}\eta,
\end{aligned}$$

the variational form of the exterior problem reads: Find $u_s \in W^2(\Omega_{ext}^{(\xi,\eta)})$ such that for all $v \in H^1_\pi(\eta_{min}, \eta_{max})$ and all $\xi \in \mathbb{R}_+$

$$a_0(v, u_s) + a_1(v, \partial_\xi u_s) + a_2(v, \partial_\xi^2 u_s) = 0, \quad (12)$$

$$u_s(0, \eta) = u_D(\eta), \quad (13)$$

$$\partial_\xi u_s(0, \eta) = u_N(\eta). \quad (14)$$

Here $H^1_\pi(\eta_{min}, \eta_{\max})$ is the subspace of periodic functions in $H^1([\eta_{min}, \eta_{max}])$.

The function space $W^2(\Omega_{ext}^{(\xi,\eta)})$ is defined as

$$W^2(\Omega_{ext}^{(\xi,\eta)}) = \left\{ \begin{array}{l} w(\xi_0,\eta) \in H^1_\pi(\eta_{min},\eta_{max}) : \forall \xi_0 \in \mathbb{R}, \\ w(\xi,\eta_0) \in C^2(\mathbb{R}_+) : \forall \eta_0 \in [\eta_{min},\eta_{max}] \end{array} \right\}.$$

The coupling between interior and exterior problem is determined by (13) and (14). We now perform a semi discretization in η.

The fields u_s and u_{inc} are approximated by

$$u_s^h(\xi,\eta) = \sum_{j=1}^{N_B} u_{s,j}^h(\xi)\psi_j(\eta) \quad \text{and} \quad u_{inc}^h(\xi,\eta) = \sum_{j=1}^{N_B} u_{inc,j}^h(\xi)\psi_j(\eta), \tag{15}$$

where $\{\psi_1, ..., \psi_{N_B}\}$ is a basis of $S_h \subset H^1_\pi(\eta_{min},\eta_{max})$. The space S_h is the trace space of the finite element space V_h of the interior problem. The coefficient-vector of $u_s^h(\xi,\eta)$ is denoted by $\boldsymbol{u}_s^h(\xi)$. Inserting (15) in (12) for u_s yields the system

$$A_0(\xi)\boldsymbol{u}_s^h(\xi) + A_1(\xi)\partial_\xi \boldsymbol{u}_s^h(\xi) + A_2(\xi)\partial_\xi^2 \boldsymbol{u}_s^h(\xi) = 0. \tag{16}$$

4 Computation of local matrices in the semi-discrete exterior system

We compute local contributions to the matrices A_0, A_1, A_2 in (16) for the simple case of linear C^0-elements. The generalization to higher order elements is straightforward.

The system matrices A_0, A_1 and A_2 from (16) are given by

$$A_{2,ij}\partial_{\xi\xi}u_{s,j}^h := a_2(\psi_i,\psi_j)\partial_{\xi\xi}u_{s,j}^h = \left(\int_{\Gamma_\eta} \psi_i F_{11}\psi_j d\eta\right)\partial_{\xi\xi}u_{s,j}^h,$$

$$\begin{aligned} A_{1,ij}\partial_\xi u_{s,j}^h :=& a_1(\psi_i, \psi_j\partial_\xi u_{s,j}^h) \\ =& \left(\int_{\Gamma_\eta} \psi_i(\partial_\xi F_{11}\psi_j + F_{12}\partial_\eta\psi_j)\mathrm{d}\eta - \int_{\Gamma_\eta} \partial_\eta\psi_i F_{21}\psi_j \mathrm{d}\eta\right)\partial_\xi u_{s,j}^h, \\ A_{0,ij}u_{s,j}^h :=& a_0(\psi_i, \psi_j u_{s,j}^h) \\ =& \left(\int_{\Gamma_\eta} \psi_i\partial_\eta\psi_j\partial_\xi F_{12} - \partial_\eta\psi_i\partial_\eta\psi_j F_{22} + |J|k^2\psi_i\psi_j \mathrm{d}\eta\right) u_{s,j}^h. \end{aligned}$$

On a segment $Q_q^{(\xi,\eta)}$ the two linear basis functions are given by

$$v_1(\eta) = \frac{\eta_{q+1} - \eta}{\eta_{q+1} - \eta_q}, \quad v_2(\eta) = \frac{\eta - \eta_q}{\eta_{q+1} - \eta_q}. \tag{17}$$

Local contributions from Segment Q_q are

$$
\begin{aligned}
(A_2^{(q)})_{ij} &= \int_{\eta_q}^{\eta_{q+1}} v_i v_j F_{11} \mathrm{d}\eta, \\
(A_1^{(q)})_{ij} &= \int_{\eta_q}^{\eta_{q+1}} (v_i v_j \partial_\xi F_{11} + v_i \partial_\eta v_j F_{12} - \partial_\eta v_i v_j F_{21}) \mathrm{d}\eta, \\
(A_0^{(q)})_{ij} &= \int_{\eta_q}^{\eta_{q+1}} (v_i \partial_\eta v_j \partial_\xi F_{12} - \partial_\eta v_i \partial_\eta v_j F_{22} + v_i v_j |J| k_q^2) \mathrm{d}\eta,
\end{aligned}
\tag{18}
$$

for $i, j \in \{1, 2\}$. Here k_q is the wavenumber, which is assumed to be constant in segment Q_q. To compute these matrices it is necessary to derive the transformations $B_q^{loc} : Q_q^{(\xi,\eta)} \to Q_q^{(x,y)}$.

The following derivation is done for the first segment $q = 1$, therefore we drop the subscript 1 in what follows. The segment (cf. Fig. 7) is bounded by two

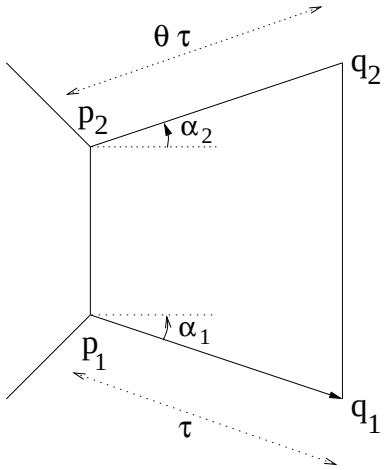

Fig. 7. Segment $Q_1^{(x,y)}$.

rays $\overline{\boldsymbol{p}_1\boldsymbol{q}_1}$ respectively $\overline{\boldsymbol{p}_2\boldsymbol{q}_2}$, with parameter representations

$$
\boldsymbol{g}_1(\tau) = \boldsymbol{p}_1 + \tau \boldsymbol{e}_1, \ \boldsymbol{g}_2(\tau) = \boldsymbol{p}_2 + \theta\tau \boldsymbol{e}_2, \tag{19}
$$

where $\boldsymbol{e}_1$, $\boldsymbol{e}_2$ are the unit vectors

$$
\boldsymbol{e}_1 = (\boldsymbol{q}_1 - \boldsymbol{p}_1)/(|\boldsymbol{q}_1 - \boldsymbol{p}_1|), \ \boldsymbol{e}_2 = (\boldsymbol{q}_2 - \boldsymbol{p}_2)/(|\boldsymbol{q}_2 - \boldsymbol{p}_2|), \tag{20}
$$

and θ is a scaling factor, obtained from the requirement that $\overline{\boldsymbol{p}_1\boldsymbol{p}_2} \parallel \overline{\boldsymbol{q}_1\boldsymbol{q}_2}$. Hence from $\theta\tau \cos\alpha_2 = \tau \cos\alpha_1$ we get $\theta = \cos\alpha_1 / \cos\alpha_2$. We define ξ as the distance between the lines $\overline{\boldsymbol{p}_1\boldsymbol{p}_2}$ and $\overline{\boldsymbol{q}_1\boldsymbol{q}_2}$, $\xi := \tau \cos\alpha_1$. This yields a symmetric parameter representation for the rays,

$$
\boldsymbol{g}_1(\xi) = \boldsymbol{p}_1 + \frac{\xi}{\zeta \cos\alpha_1}\boldsymbol{e}_1, \quad \boldsymbol{g}_2(\xi) = \boldsymbol{p}_2 + \frac{\xi}{\zeta \cos\alpha_2}\boldsymbol{e}_2. \tag{21}
$$

with $\xi \geq 0$ and a scaling factor ζ that may vary from segment to segment. If ζ and α_1 correspond to an arbitrary segment and ζ_p and $\alpha_{2,p}$ to the pre-

vious segment, setting $\zeta = \zeta_p \cos\alpha_{2,p}/\cos\alpha_1$ ensures that these two segments fit continuously. The transformation between the $\xi\eta$- and the xy-coordinate system is

$$\begin{pmatrix} x \\ y \end{pmatrix} = \boldsymbol{g}_1(\xi) + \frac{\eta - \eta_1}{\eta_2 - \eta_1}(\boldsymbol{g}_2(\xi) - \boldsymbol{g}_1(\xi)). \tag{22}$$

With $\boldsymbol{e}_1 = (\cos\alpha_1, -\sin\alpha_1)$ and $\boldsymbol{e}_2 = (\cos\alpha_2, \sin\alpha_2)$ the mapping B^{loc} is given by

$$\begin{aligned} \begin{pmatrix} x \\ y \end{pmatrix} =: B^{loc}(\xi,\eta) = \left(1 - \frac{\eta - \eta_1}{\eta_2 - \eta_1}\right)\left(\begin{pmatrix} x_1 \\ y_1 \end{pmatrix} + \frac{\xi}{\zeta\cos\alpha_1}\begin{pmatrix} \cos\alpha_1 \\ -\sin\alpha_1 \end{pmatrix}\right) \\ + \frac{\eta - \eta_1}{\eta_2 - \eta_1}\left(\begin{pmatrix} x_2 \\ y_2 \end{pmatrix} + \frac{\xi}{\zeta\cos\alpha_2}\begin{pmatrix} \cos\alpha_2 \\ \sin\alpha_2 \end{pmatrix}\right). \end{aligned} \tag{23}$$

Taking into account that the Helmholtz equation is invariant under rotations we may assume without loss of generality that $x_1 = x_2 = 0$, $y_1 = 0$, $y_2 = h$, $\eta_1 = 0$ and $\eta_2 = 1$. The above mapping simplifies to

$$B^{loc}(\xi,\eta) = (1-\eta)\frac{\xi}{\zeta}\begin{pmatrix} 1 \\ -\tan\alpha_1 \end{pmatrix} + \eta\left(\begin{pmatrix} 0 \\ h \end{pmatrix} + \frac{\xi}{\zeta}\begin{pmatrix} 1 \\ \tan\alpha_2 \end{pmatrix}\right) \tag{24}$$

Using the abbreviations $a_1 = \tan\alpha_1$, $a_2 = \tan\alpha_2$ and $a = \tan\alpha_1 + \tan\alpha_2$ the Jacobian of B^{loc} is

$$J(\xi,\eta) = \begin{pmatrix} \frac{1}{\zeta} & 0 \\ -\frac{1}{\zeta}a_1 + \frac{\eta}{\zeta}a & h + \frac{\xi}{\zeta}a \end{pmatrix}. \tag{25}$$

With $|J| = (h\zeta + \xi a)/\zeta^2$ we have

$$J^{-1}(\xi,\eta) = \begin{pmatrix} \zeta & 0 \\ -\frac{\zeta(-a_1+\eta a)}{h\zeta+a\xi} & \frac{\zeta}{h\zeta+a\xi} \end{pmatrix},\ F = \begin{pmatrix} h\zeta + \xi a & a_1 - \eta a \\ a_1 - \eta a & \frac{(a_1-\eta a)^2+1}{h\zeta+\xi a} \end{pmatrix}.$$

Returning to Equation (18) all local quantities now get as an additional subscript the segment number q. Inserting the above result in (18) yields

$$A_2^{(q)} = (h_q\zeta_q + \xi a_q)\begin{pmatrix} \frac{1}{3} & \frac{1}{6} \\ \frac{1}{6} & \frac{1}{3} \end{pmatrix}, \tag{26}$$

$$A_1^{(q)} = \frac{1}{3}\begin{pmatrix} a_q & -a_{2,q} + 2a_{1,q} \\ 2a_{2,q} - a_{1,q} & a_q \end{pmatrix}, \tag{27}$$

$$A_0^{(q)} = \frac{1}{3}\frac{1}{h_q\zeta_q + \xi a_q}\begin{pmatrix} -a_{1,q}^2 + a_{1,q}a_{2,q} - a_{2,q}^2 - 3 & a_{1,q}^2 - a_{1,q}a_{2,q} + a_{2,q}^2 + 3 \\ a_{1,q}^2 - a_{1,q}a_{2,q} + a_{2,q}^2 + 3 & -a_{1,q}^2 + a_{1,q}a_{2,q} - a_{2,q}^2 - 3 \end{pmatrix} + (h_q\zeta_q + \xi a_q)\frac{k_q^2}{\zeta_q^2}\begin{pmatrix} \frac{1}{3} & \frac{1}{6} \\ \frac{1}{6} & \frac{1}{3} \end{pmatrix}. \tag{28}$$

If $\boldsymbol{u}_{s,q}^h(\xi)$ is the coefficient vector with degrees of freedom corresponding to segment Q_q, a local contribution to the left-hand side of (16) is

$$\sum_{j=0}^{2}\left(\sum_{i=-1}^{1}(h_q\zeta_q + \xi a_q)^i M^{(q)}\{i,j\}\right)\partial_\xi^j \boldsymbol{u}_{s,q}^h(\xi) = \sum_{j=0}^{2} A_j^{(q)}\partial_\xi^j \boldsymbol{u}_{s,q}^h \tag{29}$$

with

$$\begin{aligned} M^{(q)}\{-1,0\} &= \frac{1}{3}\begin{pmatrix} -a_1^2 + a_1a_2 - a_2^2 - 3 & a_1^2 - a_1a_2 + a_2^2 + 3 \\ a_1^2 - a_1a_2 + a_2^2 + 3 & -a_1^2 + a_1a_2 - a_2^2 - 3 \end{pmatrix}^{(q)}, \\ M^{(q)}\{1,0\} &= \frac{k_q^2}{\zeta_q^2}\begin{pmatrix} \frac{1}{3} & \frac{1}{6} \\ \frac{1}{6} & \frac{1}{3} \end{pmatrix}, \\ M^{(q)}\{0,1\} &= \frac{1}{3}\begin{pmatrix} a & -a_2 + 2a_1 \\ 2a_2 - a_1 & a \end{pmatrix}^{(q)}, \\ M^{(q)}\{1,2\} &= \frac{1}{3}\begin{pmatrix} 1 & \frac{1}{2} \\ \frac{1}{2} & 1 \end{pmatrix}, \end{aligned} \tag{30}$$

and all other matrices $M^{(q)}\{i,j\} = 0$.

5 Semi-discrete PML system

The PML method is based on a complex continuation in the radial like variable ξ to right complex half plane. As can be seen in (30) the entries of the globally assembled matrices $A_0(\xi)$, $A_1(\xi)$, $A_2(\xi)$ are composed of rational expressions in ξ. Due to $\zeta_q h_q > 0$ and $a_q > 0$, there is no pole for a complex ξ with $\Re(\xi) > 0$. This guarantees analyticity of the matrices in right complex plane. Therefore a solution of (16) has a complex continuation $\boldsymbol{u}_s^h(z)$, *cf.* [15]. Motivated by the case of a homogeneous exterior domain we expect an exponential damping of the solution for $\Im(z) \to +\infty$.

The PML method is realized by replacing the variable ξ in (16) with $\gamma\xi$, $\Re\gamma >$

$0, \Im\gamma > 0$, and by replacing the unbounded domain Ω_{ext} with the bounded domain $\Omega_{\mathrm{PML}} := \{(\xi,\eta) \in \Omega_{ext} : \xi \in [0,\rho]; \eta \in [\eta_{min}, \eta_{max}]\}$. Because of the expected absorbing character of the PML-layer we impose a zero Dirichlet boundary condition on the outer boundary $\xi = \rho$. With

$$\gamma = 1 + i\sigma\,,\ \sigma > 0 \text{ and } \boldsymbol{u}_{\mathrm{PML}}(\xi) := \boldsymbol{u}_s^h(\gamma\xi), \tag{31}$$

the PML system is determined by

$$A_0(\gamma\xi)\boldsymbol{u}_{\mathrm{PML}}(\xi) + A_1(\gamma\xi)\frac{1}{\gamma}\partial_\xi \boldsymbol{u}_{\mathrm{PML}}(\xi) + A_2(\gamma\xi)\frac{1}{\gamma^2}\partial_\xi^2 \boldsymbol{u}_{\mathrm{PML}}(\xi) = 0. \tag{32}$$

Remark 4 *Instead of choosing the complex coordinate stretching $\xi \mapsto \gamma\xi$ it is possible to choose a more general coordinate transform $\xi \mapsto \gamma(\xi)$ such that $\gamma \in C^2([0,\infty))$, $\gamma(0) = 0$, see for example [16]. The condition $\Im\gamma(\xi) \to \infty$ for $\xi \to \infty$ ensures the decay of the complex continuation of an outgoing solution along the path $\gamma(\xi)$. As shown in the next section a path γ with $\gamma'(0) \neq 0$ leads to a jump in the Neumann derivative on the transparent boundary which is easily incorporated in a finite element discretization. In our numerical experiments we could not improve the performance significantly using more elaborated paths. Moreover, from our point of view this only increases the number of parameters to adjust.*

Remark 5 *The pole condition approach is a general concept to define transparent boundary condition even on inhomogeneous exterior domains. A solution $u_s(\xi,\eta)$ to the Helmholtz equation satisfies the pole condition if its Laplace transform along rays joining the exterior boundary with infinity is holomorphic in the lower complex half plane. This characterizes outgoing waves. We detail the numerical implementation of the pole condition for the semi discrete system (16) in a succeeding paper. In [14] we have shown for radial symmetric exterior domains that a solution satisfying the pole condition admits a complex continuation which decays exponentially fast on the straight line $(1+i\sigma)\xi$. This leads to a convergence proof of the PML-method. We hope that an analogous result holds true in our semi-discrete setting.*

6 Complete discretization by the finite element method

With the complex extension of the PML-method, the left-hand side of (29) reads

$$\sum_{j=0}^{2}\Big(\sum_{i=-1}^{1}(h_q\zeta_k + (\gamma\xi)a_q)^i\, M^{(q)}\{i,j\}\Big)(1/\gamma)^j\ \partial_\xi^j \boldsymbol{u}_{\mathrm{PML},q}(\xi). \tag{33}$$

We discretize the semi-discrete problem (32) by finite elements in ξ. Since $\boldsymbol{u}_{\mathrm{PML},q}(\xi)$ is analytic in ξ, different numerical techniques to discretize in ξ such as spectral methods are promising.

The m'th component of $\boldsymbol{u}_{\mathrm{PML},q}(\xi)$, $m' = 1, 2$, is approximated by

$$u^h_{\mathrm{PML},q,m'}(\xi) = \sum_{n'=1}^{N_\xi} c_{\mathrm{PML},q,m'n'} \Phi_{n'}(\xi), \tag{34}$$

where $\{\Phi_1, ...\Phi_{N_\xi}\}$ is a basis of the finite element space $X_h \subset H^1([0,\rho])$, i.e. N_ξ is the number of one-dimensional finite elements in direction ξ in the PML. We may interpret the resulting complete discretization of the exterior problem as a two dimensional finite element discretization on quadrilaterals. Their quality depends on the initial choice of the rays in Section 2. Hence it is favorable to choose $c_i \approx c_k$ in the construction of the generalized normal rays on page 5. As the solution in the PML is analytic in direction ξ, it is advantageous to choose a higher order finite element space for X_h.

Additional degrees of freedom $n_{\mathrm{PML},q,m'}$ are introduced on the boundary $\partial\Omega$ by

$$n_{\mathrm{PML},q,m'} = \partial_\xi u^h_{\mathrm{PML},q,m'}(0). \tag{35}$$

Multiplying (33) by the test functions $\Phi_n \boldsymbol{e}_m$ for $m = 1, 2$ and integrating over the layer in ξ-direction yields after an integration by parts

$$\sum_{m'=1}^{2} \sum_{n'=1}^{N_\xi} (S^q_{mn,m'n'} + D^q_{mn,m'n'} + M^q_{mn,m'n'}) c_{\mathrm{PML},q,m'n'} + \sum_{m'=1}^{2} R^q_{mn,m'} n_{\mathrm{PML},q,m'} \tag{36}$$

with

$$S^q_{mn,m'n'} = -M^{(q)}_{mm'}\{1,2\} \int_0^\rho \frac{1}{\gamma^2}(h_q\zeta_q + (\gamma\xi)a_q)\partial_\xi\Phi^*_n\partial_\xi\Phi_{n'}\mathrm{d}\xi, \tag{37}$$

$$\begin{aligned} D^q_{mn,m'n'} =& M^{(q)}_{mm'}\{0,1\} \int_0^\rho \frac{1}{\gamma}\Phi^*_n\partial_\xi\Phi_{n'}\mathrm{d}\xi \\ &- M^{(q)}_{mm'}\{1,2\} \int_0^\rho \frac{1}{\gamma}a_q\Phi^*_n\partial_\xi\Phi_{n'}\mathrm{d}\xi \end{aligned} \tag{38}$$

$$\begin{aligned} M^q_{mn,m'n'} =& M^{(q)}_{mm'}\{-1,0\} \int_0^\rho (h_q\zeta_q + (\gamma\xi)a_q)^{-1}\Phi^*_n\Phi_{n'}\mathrm{d}\xi \\ &+ M^{(q)}_{mm'}\{1,0\} \int_0^\rho (h_q\zeta_q + (\gamma\xi)a_q)\Phi^*_n\Phi_{n'}\mathrm{d}\xi, \end{aligned} \tag{39}$$

$$R^q_{mn,m'} = \left[\frac{1}{\gamma^2}(h_q\zeta_q + \gamma\xi)M^{(q)}_{mm'}\{1,2\}\Phi^*_n\right]_0^\rho. \tag{40}$$

Assembling (36) to a global system yields

$$(S + D + M)\boldsymbol{c}_{\mathrm{PML}} + R\boldsymbol{n}_{\mathrm{PML}} = 0. \tag{41}$$

The discrete interior problem reads: Seek u^h in $V_h = \mathrm{span}\{\varphi_1, ..., \varphi_{N_I}\} \subset$

$H^1(\Omega)$ such that

$$\begin{aligned}&\int_\Omega \nabla u^h(\boldsymbol{x})\cdot\nabla\varphi_i(\boldsymbol{x})\mathrm{d}\boldsymbol{x} - \int_\Omega k^2(\boldsymbol{x})u^h(\boldsymbol{x})\varphi_i(\boldsymbol{x})\mathrm{d}\boldsymbol{x} - \int_{\partial\Omega}\partial_n u_s^h(\boldsymbol{x})\varphi_i(\boldsymbol{x})\mathrm{d}s\\ &= \int_{\partial\Omega}\partial_n u_{inc}^h(\boldsymbol{x})\varphi_i(\boldsymbol{x})\mathrm{d}s \quad \text{for } i=1,...,N_I.\end{aligned} \tag{42}$$

The coefficient vector of u^h relative to V_h is denoted by $U=\{U_1,...,U_{N_I}\}$, hence $u^h(\boldsymbol{x})=\sum_{i=1}^{N_I}U_i\varphi_i(\boldsymbol{x})$ The exterior and the interior problem couple via the boundary integral on the left-hand side of (42). Let $\pi:\{1,...,N_B\}\to\{1,...,N_I\}$ be a mapping from the degrees of freedom corresponding to $\partial\Omega$ to the global numbering of degrees of freedom in the discrete interior problem. A local contribution of the boundary term for segment Q_q is

$$\begin{aligned}\int_{p_q}^{p_{q+1}}\partial_n u_s^h(\boldsymbol{x})\varphi_{\pi(i)}(\boldsymbol{x})\mathrm{d}s &= \int_{p_q}^{p_{q+1}}\varphi_{\pi(i)}(\boldsymbol{x})\boldsymbol{n}(\boldsymbol{x})\nabla_{xy}u_s^h(\boldsymbol{x})\mathrm{d}s\\ &= \sum_{j=q}^{q+1}\int_{\eta_q}^{\eta_{q+1}}\psi_i(\eta)(1,0)J^{-T}\nabla_{\xi\eta}(u_{s,j}^h(0)\psi_j(\eta))\mathrm{d}\eta\\ &= \sum_{j=q}^{q+1}\Bigg(\int_{\eta_q}^{\eta_{q+1}}\psi_i(\eta)(J^{-T})_{11}\psi_j(\eta)\mathrm{d}\eta\;\partial_\xi u_{s,j}^h(0)\\ &\quad+\int_{\eta_q}^{\eta_{q+1}}\psi_i(\eta)(J^{-T})_{12}\partial_\eta\psi_j(\eta)\mathrm{d}\eta\;u_{s,j}^h(0)\Bigg).\end{aligned} \tag{43}$$

Assembling the local contributions in (43) to global matrices B_1 and B_0, the boundary integrals can be expressed in vector notation as

$$\begin{pmatrix}\int_{\partial\Omega}\partial_n u_s^h(\boldsymbol{x})\varphi_{\pi(1)}(\boldsymbol{x})\mathrm{d}s\\ \vdots\\ \int_{\partial\Omega}\partial_n u_s^h(\boldsymbol{x})\varphi_{\pi(N_B)}(\boldsymbol{x})\mathrm{d}s\end{pmatrix} = B_0\begin{pmatrix}U_{\pi(1)}-u_{inc,1}(0)\\ \vdots\\ U_{\pi(N_B)}-u_{inc,N_B}(0)\end{pmatrix}+\frac{1}{\gamma}B_1\begin{pmatrix}n_{\mathrm{PML},1}\\ \vdots\\ n_{\mathrm{PML},N_B}\end{pmatrix}. \tag{44}$$

We set U_{inc} the coefficient vector of the incoming field relative to S_h, i.e $u_{inc}(x)|_{\partial\Omega}\approx\sum_{j=1}^{N_B}u_{inc,j}(0)\psi_j(\eta)$, *cf.* (15). Let P be the matrix corresponding to the mapping π. Using the above defined vectors, matrices and a vector representation of the right-hand side in (42) according to (44) with u_s^h replaced

by u_{inc}, the discrete interior problem reads

$$\begin{aligned}
&\sum_{j=1}^{N_I}\Bigg(\underbrace{\int_\Omega \nabla\varphi_i(\boldsymbol{x})\cdot\nabla\varphi_j(\boldsymbol{x})\mathrm{d}\boldsymbol{x}-\int_\Omega k^2(\boldsymbol{x})\varphi_i(\boldsymbol{x})\varphi_j(\boldsymbol{x})\mathrm{d}\boldsymbol{x}}_{K_{ij}}\Bigg)U_j\\
&-\sum_{j=1}^{N_I}\sum_{k=1}^{N_B}P_{ik}\sum_{l=1}^{N_B}B_{0,kl}(P^T)_{lj}U_j-\sum_{k=1}^{N_B}P_{ik}\frac{1}{\gamma}\sum_{l=1}^{N_B}B_{1,kl}n_{PML,l} \qquad (45)\\
&=\underbrace{\sum_{k=1}^{N_B}P_{ik}\sum_{l=1}^{N_B}B_{1,kl}\partial_\xi u^h_{inc,l}(0)}_{g_i}.
\end{aligned}$$

The decomposition $u(\boldsymbol{x})|_{\partial\Omega}=u_{inc}(\boldsymbol{x})|_{\partial\Omega}+u_s(\boldsymbol{x})|_{\partial\Omega}$ requires

$$P^TU=Qc_{\mathrm{PML}}+U_{inc}, \qquad (46)$$

where $\tilde{c}_{\mathrm{PML}}=Qc_{\mathrm{PML}}$ are the degrees of freedom in c_{PML} corresponding to $\partial\Omega$ and U_{inc} are the degrees of freedom of the incoming field on the boundary. Gathering together (41), (45) and (46) yields the global system

$$\begin{pmatrix} K-PB_0P^T & 0 & -\frac{1}{\gamma}PB_1\\ 0 & S+D+M & R\\ P^T & -Q & 0\end{pmatrix}\begin{pmatrix}U\\ c_{\mathrm{PML}}\\ n_{\mathrm{PML}}\end{pmatrix}=\begin{pmatrix}g\\ 0\\ U_{inc}\end{pmatrix}. \qquad (47)$$

This system can be further simplified. In (47) the coupling conditions between the exterior and the interior problem appear explicitly. This resembles a domain decomposition approach. In the following we will show that the additional degrees of freedom on the boundary can be avoided. The resulting system (54) also arises from a finite element system based on mixed triangular and quadrilateral elements. In this case we scale the PML-equation by γ to incorporate the matching of the exterior-interior Neumann data as a natural boundary condition. Let the degrees of freedom of the PML-layer be arranged as

$$c_{\mathrm{PML}}=\begin{pmatrix}\tilde{c}_{\mathrm{PML}}\\ c'_{\mathrm{PML}}\end{pmatrix}. \qquad (48)$$

Accordingly we split $A:=S+D+M$ as

$$A=\begin{pmatrix}A_{11} & A_{12}\\ A_{21} & A_{22}\end{pmatrix}. \qquad (49)$$

We scale the PML equation with $-\gamma$

$$\begin{pmatrix} K - PB_0P^T & 0 & -\frac{1}{\gamma}PB_1 \\ 0 & -\gamma \begin{bmatrix} A_{11} & A_{12} \\ A_{21} & A_{22} \end{bmatrix} & -\gamma R \\ 0 & & 0 \\ P^T & -Q & 0 \end{pmatrix} \begin{pmatrix} U \\ \tilde{c}_{\mathrm{PML}} \\ c'_{\mathrm{PML}} \\ n_{\mathrm{PML}} \end{pmatrix} = \begin{pmatrix} g \\ 0 \\ 0 \\ U_{inc} \end{pmatrix} \tag{50}$$

and use

$$\tilde{c}_{\mathrm{PML}} = P^T U - U_{inc} \tag{51}$$

to obtain the equivalent system

$$\begin{pmatrix} K - PB_0P^T & 0 & -\frac{1}{\gamma}PB_1 \\ -\gamma \begin{bmatrix} A_{11}P^T \\ A_{21}P^T \end{bmatrix} & -\gamma \begin{bmatrix} A_{12} \\ A_{22} \end{bmatrix} & -\gamma R \\ & & 0 \end{pmatrix} \begin{pmatrix} U \\ c'_{\mathrm{PML}} \\ n_{\mathrm{PML}} \end{pmatrix} = \begin{pmatrix} g \\ -\gamma A_{11}U_{inc} \\ -\gamma A_{21}U_{inc} \end{pmatrix}. \tag{52}$$

Performing elementary row operations yields

$$\begin{pmatrix} K - PB_0P^T - \gamma PA_{11}P^T & -\gamma PA_{12} & -\frac{1}{\gamma}PB_1 - P\gamma R \\ -\gamma A_{21}P^T & -\gamma A_{22} & 0 \\ -\gamma PA_{11}P^T & -\gamma PA_{12} & -\gamma P\tilde{R} \end{pmatrix} \begin{pmatrix} U \\ c'_{\mathrm{PML}} \\ n_{\mathrm{PML}} \end{pmatrix} = \begin{pmatrix} g - \gamma PA_{11}U_{inc} \\ -\gamma A_{21}U_{inc} \\ -\gamma PA_{11}U_{inc} \end{pmatrix}. \tag{53}$$

Since $-\frac{1}{\gamma}PB_1 - P\gamma R = 0$, according to (40) and (44), U and c'_{PML} can be determined by solving the reduced system

$$\begin{pmatrix} K - PB_0P^T - \gamma PA_{11}P^T & -\gamma PA_{12} \\ -\gamma A_{21}P^T & -\gamma A_{22} \end{pmatrix} \begin{pmatrix} U \\ c'_{\mathrm{PML}} \end{pmatrix} = \begin{pmatrix} g - \gamma PA_{11}U_{inc} \\ -\gamma A_{21}U_{inc} \end{pmatrix}. \tag{54}$$

7 Numerical examples

The scattering problem (3)-(6) is solved for two different examples with known exact solution in order to investigate the convergence of the computed solution in dependence of the thickness ρ of the PML layer. In general it is a difficult

task to verify the expected exponential convergence behavior in a numerical experiment. Since the finite element method converges only polynomially, the discretization error asymptotically dominates the error caused by the finite thickness of the PML-layer. We therefore carry out a special discrete convergence check for the quality of the transparent boundary condition. We solve a sequence of discrete problems with fixed interior triangulation and a discretization in the PML-layer given by $\xi = [0 : h_{\mathrm{PML}} : jh_{\mathrm{PML}}]$. Here h_{PML} is the mesh width in ξ-direction and jh_{PML} is the thickness of the PML-layer. Then we expect that the computed solution $u_{h,j}$ of the interior domain converges exponentially to $u_{h,\infty}$ for $j \to \infty$. We repeat this experiment for a halved mesh width in the interior domain together with the refinement $h_{PML} := h_{PML}/2$. In all the experiments we set the damping parameter in the PML $\sigma = 1$.

7.1 Infinite waveguide

In the first experiment we demonstrate, that the proposed PML can handle waveguide-like exterior inhomogeneities and polygonal computational domains. We solve a waveguide scattering problem for the case of TM-polarization, *cf.* Equation (2). Waveguides are structures with a permittivity ϵ constant in one spatial direction. Hence we can choose a $(x, y)-$ coordinate system such that ϵ is only a function of x. For a solution $\psi \in H^1(\mathbb{R})$ to the one-dimensional eigenvalue problem

$$\partial_{xx}\psi(x) + k(x)^2\psi(x) = \beta^2\psi(x)$$

with $k(x)^2 = \epsilon(x)\omega^2/c^2$, $u(x, y) = \psi(x)\exp(i\beta y)$ solves the TM-Helmholtz equation. If $\beta \in \mathbb{R}_+$ the field travels undamped along the $y-$axis and is called a *guided mode*. Note that such a solution does not obey the Sommerfeld radiation condition. As an example, consider a step index waveguide with

$$k(x)^2 = \begin{cases} k_2^2 & \text{for } |x| < d \\ k_1^2 & \text{for } |x| \geq d \end{cases} \tag{55}$$

Here $2d$ is the width of the waveguide and we assume $k_2^2 > k_1^2$. The fundamental mode u – which may not exist – corresponding to an eigenfunction $\psi(x) \in H^1(\mathbb{R})$ with maximal β^2 is given by

$$u(x, y) = \begin{cases} \left(\mathrm{e}^{i\sqrt{k_2^2-\beta^2}x} + \mathrm{e}^{-i\sqrt{k_2^2-\beta^2}x}\right)\mathrm{e}^{i\beta y} & \text{for } |x| < d \\ C\mathrm{e}^{\sqrt{-k_1^2+\beta^2}x}\mathrm{e}^{i\beta y} & \text{for } x \leq -d \\ C\mathrm{e}^{-\sqrt{-k_1^2+\beta^2}x}\mathrm{e}^{i\beta y} & \text{for } x \geq d \end{cases} \tag{56}$$

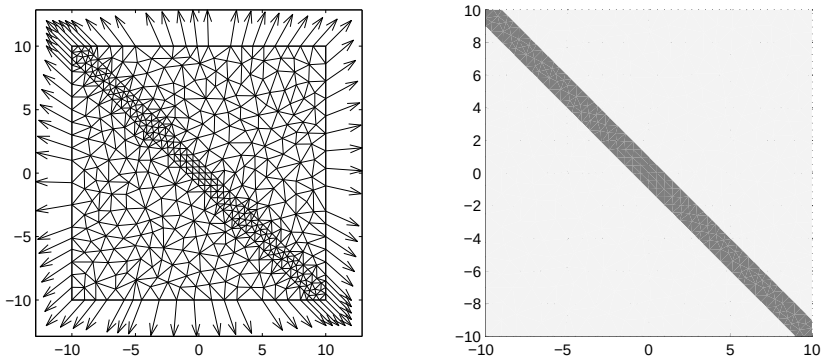

Fig. 8. Discretization of the interior domain and rays in the exterior domain (left picture). Geometry with representation of the refractive index distribution (right picture). Infinite waveguide: $k_2 = 1.32$, background: $k_1 = 0.29$.

where $C = (\exp(i\sqrt{k_2^2 - \beta^2}d) + \exp(-i\sqrt{k_2^2 - \beta^2}d))/\exp(-\sqrt{k_1^2 + \beta^2}d)$. The fundamental mode decays exponentially fast for $|x| \to \infty$. In the numerical experiment we choose $d = 1/\sqrt{2}$, $k_1 = 0.29$ and $k_2 = 1.32$. This yields a fundamental mode with $\beta = 0.8767339289\ldots$.

As depicted in Fig. 8 the computational domain is the square $[-10, 10] \times [-10, 10]$ with the waveguide connecting two opposite corners. The incoming field in the global system (54) is only specified along the left and upper side of the computational domain by setting $U_{inc} = u$ and $g = \partial_\xi u$.

In a first setting we use a very fine discretization of the interior domain and the PML layer. We want to study the convergence to the analytic solution when increasing the thickness of the PML layer. Fig. 9 shows a semilog plot of the relative error $e_1 := ||u - u_h||_2/||u||_2$ in dependence of the thickness ρ of the PML-layer. For a small thickness of the PML-layer and a huge number of degrees of freedom in the finite element discretization the error caused by the finite thickness of the PML-layer dominates. Here the error e_1 decays exponentially with respect to ρ. With growing thickness of the PML-layer the discretization error becomes more and more relevant. From $\rho = 2$ for linear elements and $\rho = 4$ for quadratic elements a further increase of ρ has no influence on the error.

In the second setting we study convergence to the discrete solution $u_{h,\infty}$ as described at the beginning of this section. Here $u_{h,j}$ is calculated using linear finite elements. The discrete system is characterized by the number of discretization points per wavelength ($\mathrm{PpW}_{\mathrm{int}}$) in the interior domain and h_{PML} in the PML-layer. Fig. 10 shows a semilog plot of the sequence $e_2(j) = ||u_{h,J} - u_{h,j}||_2/||u_{h,J}||_2$ versus the thickness of the PML-layer $\rho = jh_{PML}$ for different choices of $\mathrm{PpW}_{\mathrm{int}}$ and h_{PML}. For sure the converged discrete solution $u_{h,\infty}$ is not available an we have therefore replaced it by $u_{h,J}$ with $J = 20/h_{PML}$. The sequence converges exponentially with respect to ρ. For

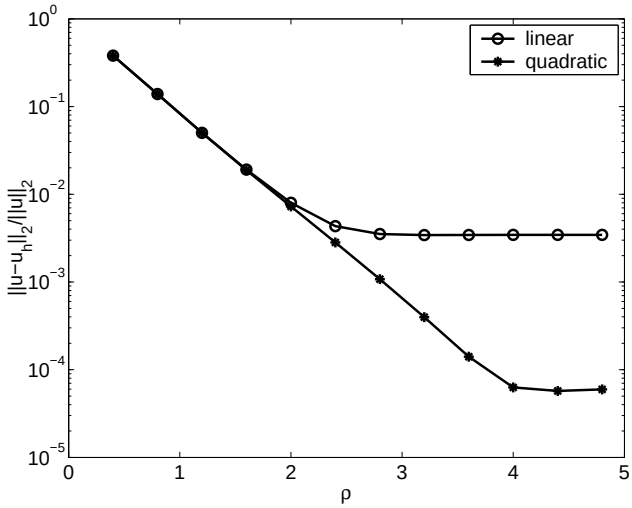

Fig. 9. Relative error $||u - u_h||_2/||u||_2$ versus thickness of the PML-layer for linear and quadratic finite elements in the first experiment.

small ρ we observe the same convergence behavior as in Fig. 9.

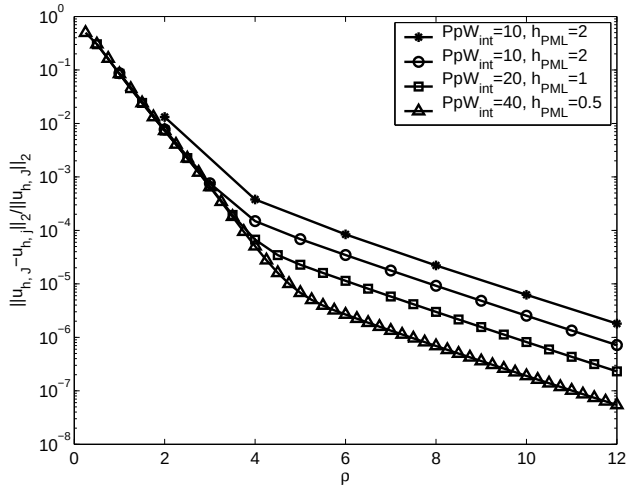

Fig. 10. Relative error $e_2(j) = ||u_{h,J} - u_{h,j}||_2/||u_{h,J}||_2$ for different numbers of degrees of freedom in the linear finite element discretization (increasing from top to down) in the first experiment. The discretization is such that there are at least PpW_{int} points per wave-length in the computational domain.

7.2 Scattering by a cylinder

In the second experiment we solve a cylinder scattering problem for the case of TM-polarization, with zero boundary condition for the electric field on the surface of the cylinder. The geometry is depicted in Fig. 11. The electric field is computed in a square region with a circular hole of radius 1 ($[-1.5, 1.5] \times [-1.5, 1.5] \setminus B_1(0, 0)$) with linear and quadratic finite elements.

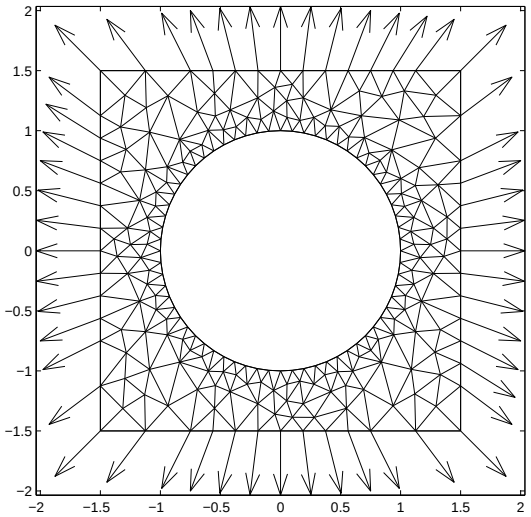

Fig. 11. Discretization of the interior domain and rays in the exterior domain.

Again, in the first setting we use a fine discretization in the computational domain and the PML layer. Fig. 12 shows a semilog plot of the relative error $e_1 := ||u - u_h||_2/||u||_2$ in dependence of the thickness ρ of the PML-layer. Again there is an exponential decay of the error e_1 with ρ in the range where the error caused by the finite thickness of the PML-layer dominates. This time quadratic finite elements lead to a better rate in the semilog plot.

Fig. 13 shows a semilog plot of the sequence $e_2(j) = ||u_{h,J} - u_{h,j}||_2$ in dependence of the thickness of the PML-layer $\rho = jh_{PML}$. Again we replace $u_{h,\infty}$ by $u_{h,J}$ with $J := 20/h_{PML}$. The sequence shows the same exponential decay as in the first experiment.

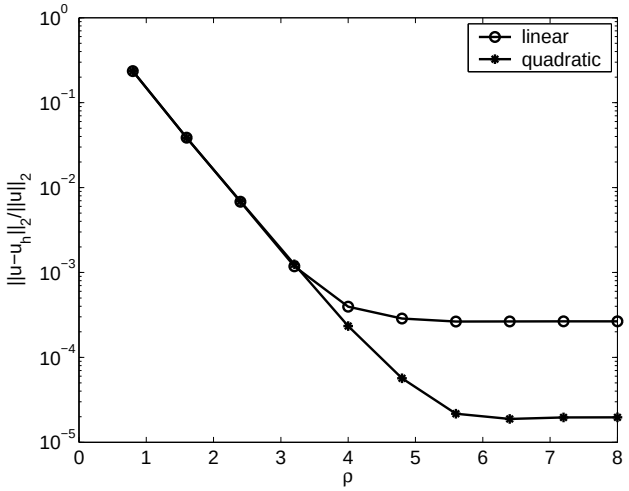

Fig. 12. Relative error $||u - u_h||_2/||u||_2$ versus thickness of the PML-layer for linear and quadratic finite elements in the second experiment.

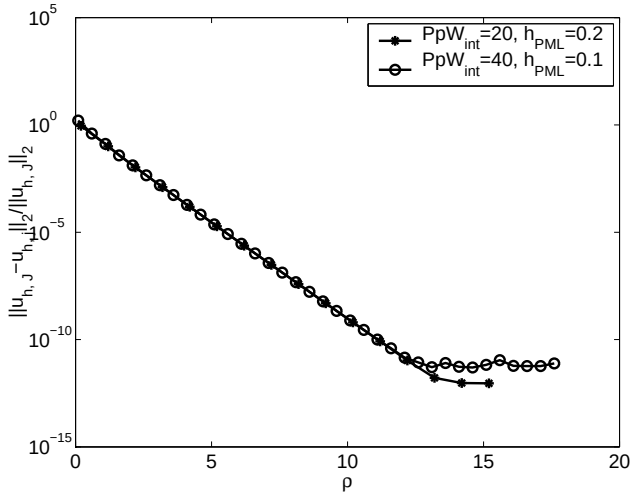

Fig. 13. Relative error $e_2(j) = ||u_{h,J} - u_{h,j}||_2/||u_h(\infty)||_2$ for different numbers of degrees of freedom in the linear finite element discretization (increasing from top to down, determined by the points per wavelength (PpW))) in the second experiment.

8 Conclusions

The PML-method has been formulated in the context of F. Schmidt's discretization scheme of the exterior domain [12]. This provides a tool for solving scattering problems with inhomogeneous exterior domains in the case, where the refraction index distribution allows to choose a decomposition in segments with constant refractive index. Numerical experiments have indicated exponential decay of the error $||u - u(\rho)||_2$ with respect to the thickness ρ of the PML-layer.

Acknowledgments

We thank P. Deuflhard for support and discussions. We acknowledge support by the initiative *DFG Research Center* MATHEON *"Mathematics for key technologies"* and by the German Federal Ministry of Education and Research, BMBF, under contract no. 13N8252 (*"HiPhoCs"*).

References

[1] J. Bérenger, A perfectly matched layer for the absorption of electromagnetic waves, J. Comput. Phys. 114 (2) (1994) 185–200.

[2] W. Chew, W. Weedon, A 3-D Perfectly Matched Medium from Modified

Maxwell's Equations with Stretched Coordinates, Micro. Opt. Tech. Lett. 7 (13) (1994) 599–604.

[3] W. Chew, W. Weedon, A 3-D Perfectly Matched Medium by Coordinate Stretching and Its Absorption of Static Fields, in: Applied Computational Electromagnetics Symposium Digist, Vol. 1, 1995, pp. 482–489.

[4] W. Chew, J. Jin, E. Michielssen, Complex Coordinate Stretching as a Generalized Absorbing Boundary Condition, unpublished.

[5] F. Collino, P. Monk, The perfectly matched layer in curvilinear coordinates, SIAM J. Sci. Comput. 19 (6) (1998) 2061–2090.

[6] M. Lassas, E. Somersalo, On the existence and convergence of the solution of PML equations., Computing No.3, 229-241 60 (3) (1998) 229–241.

[7] M. Lassas, E. Somersalo, Analysis of the PML equations in general convex geometry., Proc. R. Soc. Edinb., Sect. A, Math. 131 (5) (2001) 1183–1207.

[8] M. Kuzuoglu, R. Mittra, Investigation of Nonplanar Perfectly Matched Absorbers for Finite Element Mesh Truncation, IEEE Transaction On Antennas and Propagation 45 (2) (1997) 474–486.

[9] M. Lassas, J. Liukkonen, E. Somersalo, Complex Riemannian metric and absorbing boundary condition., J. Math. Pures Appl. 80 (7) (2001) 739–768.

[10] H. Shaker, Ein neues Verfahren zur Lösung des Streuproblems der Maxwell-Gleichungen, Master's thesis, Zuse Institute Berlin, Universität Hamburg, Fachbereich Physik. Diplomarbeit (2003).

[11] F. Ihlenburg, Finite Element Analysis of Acoustic Scattering, Springer, 1998.

[12] F. Schmidt, A New Approach to Coupled Interior-Exterior Helmholtz-Type Problems: Theory and Algorithms, Habilitation thesis, Konrad-Zuse-Zentrum Berlin, Fachbereich Mathematik und Informatik, FU Berlin (2001).

[13] T. Hohage, F. Schmidt, L. Zschiedrich, Solving time-harmonic scattering problems based on the pole condition. I: Theory., SIAM J. Math. Anal. 35 (1) (2003) 183–210.

[14] T. Hohage, F. Schmidt, L. Zschiedrich, Solving time-harmonic scattering problems based on the pole condition. II: Convergence of the PML method., SIAM J. Math. Anal. 35 (3) (2003) 547–560.

[15] W. Walter, Gewöhnliche Differentialgleichungen, Springer Verlag, 1993.

[16] E. Bécache, A.-S. Bonnet, G. Legendre, Perfectly matched layers for the convected Helmholtz equation, SIAM Journal on Numerical Analysis 42 (1) (2004) 409 – 433.